Coexistence of ferroelectricity and magnetism in transition-metal-doped n = 3 Aurivillius phases

2008 J. Phys.: Condens. Matter 20 025215

(http://iopscience.iop.org/0953-8984/20/2/025215)

J. Phys.: Condens. Matter **20** (2008) 025215 (6pp) doi:10.1088/0953-8984/20/02/025215

Coexistence of ferroelectricity and magnetism in transition-metal-doped $n = 3$ Aurivillius phases

N Sharma[1,4], B J Kennedy[1], M M Elcombe[2], Y Liu[3] and C D Ling[1,2]

[1] School of Chemistry, The University of Sydney, Sydney, NSW 2006, Australia
[2] Bragg Institute, ANSTO, PMB 1, Menai, NSW 2234, Australia
[3] Research School of Chemistry, Australian National University, Canberra, ACT 0200, Australia

Received 7 August 2007, in final form 15 October 2007
Published 6 December 2007
Online at stacks.iop.org/JPhysCM/20/025215

Abstract

Magnetic-cation-doped three-layer Aurivillius phases $Bi_{2-x}Sr_{2+x}(Nb/Ta)_{2+x}M_{1-x}O_{12}$, $x \approx 0.5$ and M = Ru^{4+}, Ir^{4+} or Mn^{4+}, are shown to have the same orthorhombic space group symmetry and similar dielectric and ferroelectric properties as their (non-magnetic) ferroelectric parent compounds $Bi_{2-x}Sr_{2+x}Nb_{2+x}Ti_{1-x}O_{12}$, $x = 0, 0.5$. The magnetic-cation-doped phases also show evidence for short-range ferromagnetic (M = Mn) and antiferromagnetic (M = Ru and Ir) exchange, demonstrating the potential of these naturally layered phases as templates for multiferroic (magnetoelectric) materials.

(Some figures in this article are in colour only in the electronic version)

1. Introduction

Aurivillius phases $[Bi_2O_2]\cdot[A_{n-1}B_nO_{3n+1}]$ are layered oxides composed of single α-PbO-type layers $[Bi_2O_2]^{2+}$ alternating with n perovskite-type layers [1, 2]. Interest in Aurivillius phases has focused on their catalytic properties and oxygen ion conductivity, as well as their strong ferroelectricity [3, 4], which arises due to the rotation of BO_6 octahedra, lowering the symmetry from tetragonal to orthorhombic or monoclinic, and allowing the perovskite A- and B-site cations to be displaced relative to the oxygen anion array.

Three-layer ($n = 3$) Aurivillius phases present the greatest contrast between the coordination environments of the B-site cations in the central and outer octahedral layers of the perovskite-type block, maximizing the potential for layered B-site ordering; although considerable B-site disorder is still observed, e.g. between Nb and Ti in $Bi_2Sr_2Nb_2TiO_{12}$ [5]. Substituting magnetic transition metal cations into the central octahedral layer of the perovskite-type block, while maintaining ferroelectric displacements in the outer octahedral layers, presents a possible route to multiferroic (magnetoelectric) materials. However, there have been few reports of Aurivillius phases that contain magnetic transition metal cations. Most of these concern high-order Aurivillius phases ($n \geqslant 4$) such as $Bi_5Ti_3FeO_{15}$, which have a strong propensity for stacking faults [6] and B-site disorder [7, 8], making long-range-ordered magnetism unlikely.

Recently we described the synthesis of three-layer ($n = 3$) Aurivillius phases $Bi_{2-x}Sr_{2+x}B_{2+x}M_{1-x}O_{12}$, where B = Nb, Ta and M = Ru^{4+}, Ir^{4+} and Mn^{4+} [9]. The magnetic cations (M) replace the B-site cation Ti^{4+} in the $Bi_2Sr_2Nb_2TiO_{12}$ parent structure. The magnetic cations were shown to predominantly occupy the central perovskite B-site layer by Rietveld refinement of variable wavelength synchrotron x-ray diffraction data making use of anomalous dispersion at the Ru and Nb K edges. However, only 50–60% ($0.4 \leqslant x \leqslant 0.5$) of the central B-site layer was substituted with magnetic cations. Higher substitutions (lower x) could not be achieved, in contrast to the reports of Yu *et al* [10] and Tripathy *et al* [11].

Here, we report evidence from Rietveld refinement of low-temperature neutron powder diffraction (NPD) data showing that the space group symmetry of these phases is lowered from tetragonal $I4/mmm$ to orthorhombic $B2cb$. A similar symmetry lowering was observed for the undoped $x = 0$ parent phase $Bi_2Sr_2Nb_2TiO_{12}$ [12]. Ferroelectric displacements and orthorhombic distortions of the BO_6 octahedra in the magnetically doped phases are compared to those observed

[4] Author to whom any correspondence should be addressed.

in the undoped parent. In combination with the evidence for short-range magnetic order from magnetic susceptibility measurements, this is the first clear report of Aurivillius phases that exhibit both magnetic exchange and ferroelectricity.

2. Experimental details

The synthesis and synchrotron x-ray powder diffraction data collection of the magnetic-cation-doped three-layer Aurivillius phases has been described previously [9]. $Bi_{2-x}Sr_{2+x}Nb_{2+x}Ti_{1-x}O_{12}$, where $x = 0$ and 0.5, were synthesized and characterized by a method adopted from the work of Hervoches and Lightfoot [5].

NPD data were collected on the High Resolution Powder Diffractometer (HRPD) at the High-Flux Australian Reactor (HIFAR) facility, Australian Nuclear Science and Technology Organization (ANSTO), Lucas Heights Science and Technology Center, Australia. NPD data were not collected for the M = Ir samples due to the high neutron absorption cross-section and high cost of iridium, both of which make it unsuitable for data collection at a low-flux source. Low-temperature NPD data were collected at ∼5 K using a liquid-helium-cooled cryostat at $\lambda = 1.49$ Å. Rietveld refinements were carried out using the GSAS [13] suite of programs with the EXPGUI [14] front-end.

In order to perform dielectric measurements, pellets of the samples were sintered at 950 °C for 4 days to ensure uniform densities greater than 90% of their theoretical density. The sintering temperature was chosen to be slightly below the synthesis temperatures (1050 °C) in order to minimize bismuth loss. The 13 mm diameter and 1–2 mm thick pellets were polished, coated on both sides with conductive silver paste and heat-treated at 550 °C for 30 min to ensure good electrical contact. The dielectric properties were then measured using a high-precision *LCR* meter (Agilent 4284A) at room temperature. The ferroelectric hysteresis loops were measured on an analyzer of electro-ceramic material and devices (Aixacct TF Analyzer 2000, Germany) at room temperature.

Magnetic property measurements were carried out on a Physical Properties Measurement System (PPMS) (Quantum Design) using the DC extraction method in an applied magnetic field of 10 000 Oe. In order to avoid the preferential alignment of these strongly anisotropic layered phases in the applied magnetic field, the samples were mixed with a small quantity of Vaseline™.

3. Results

The structures of $Bi_{2-x}Sr_{2+x}B_{2+x}M_{1-x}O_{12}$ (B = Nb, Ta and M = Ru, Ir, Mn) were initially Rietveld-refined against synchrotron x-ray diffraction data [9] in the non-ferroelectric tetragonal $I4/mmm$ symmetry as reported for $Bi_{2-x}Sr_{2+x}Nb_{2+x}Ti_{1-x}O_{12}$ [5]. However, the $x = 0$ case $Bi_2Sr_2Nb_2TiO_{12}$ has recently been shown to be symmetry-lowered to ferroelectric orthorhombic $B2cb$ symmetry by Zhou *et al* [12], using NPD data. NPD data were therefore collected for $Bi_{2-x}Sr_{2+x}B_{2+x}M_{1-x}O_{12}$ (B = Nb, Ta, M = Ru, Mn and $x \sim 0.5$) and $Bi_{2-x}Sr_{2+x}Nb_{2+x}Ti_{1-x}O_{12}$ ($x = 0$, 0.5) in order to search for evidence of the same symmetry-lowering to a ferroelectrically active symmetry.

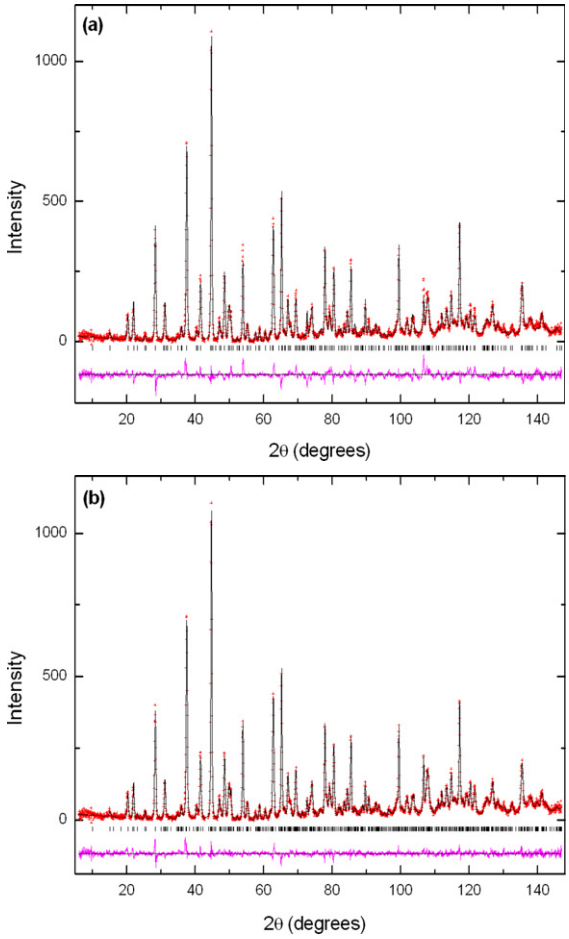

Figure 1. Final fit to Rietveld-refined low-temperature NPD ($\lambda = 1.49$ Å) data for $Bi_{2-x}Sr_{2+x}Nb_{2+x}Ru_{1-x}O_{12}$, $x = 0.5$ in (a) $I4/mmm$ and (b) $B2cb$ symmetry. Observed data are shown as crosses (+), calculated data as a solid line, and the difference as a solid line below. All refinements were performed using isotropic atomic displacement parameters.

The structure of the pure $Bi_{2-x}Sr_{2+x}Nb_{2+x}Ru_{1-x}O_{12}$, $x = 0.5$, sample was Rietveld-refined in both $I4/mmm$ and $B2cb$ symmetry in order to determine the best fit (figure 1). The final structural parameters of Rietveld refinements in $B2cb$ symmetry are shown in table 1 and the statistics of the fits are shown in table 2. Thermal ellipsoidal plots of the atomic displacement parameters (ADPs) in $I4/mmm$ and $B2cb$ symmetry are shown in figure 2. Figure 2 shows large and highly anisotropic ADPs on O1 in $I4/mmm$ symmetry, which are indicative of a symmetry-lowering mode. In comparison, the ADPs on the O1 site in $B2cb$ symmetry are far more isotropic. Further evidence of symmetry-lowering is shown in the considerable improvement of the refinement statistics in $B2cb$ symmetry (R_F^2 decreases from 8.96 to 3.76, R_p decreases from 6.61 to 4.93, wR_p decreases from 8.47 to 6.06 and goodness-of-fit χ^2 decreases from 4.23 to 2.19). The behavior of the ADPs and the improvement in refinement statistics strongly support the symmetry-lowering.

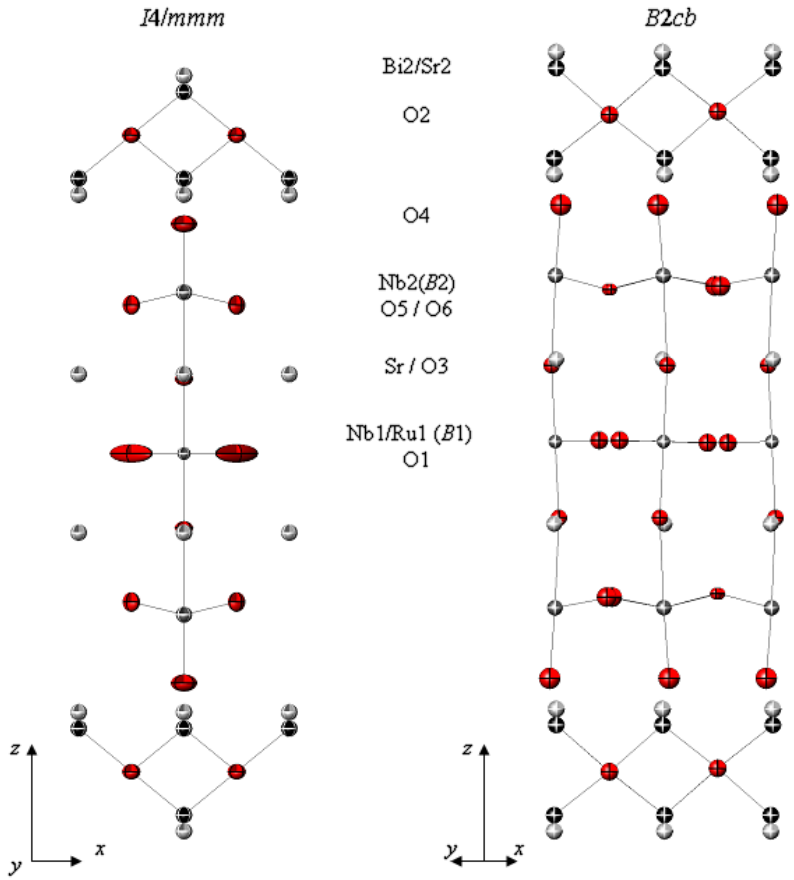

Figure 2. Thermal ellipsoid plots of final Rietveld-refined model of $Bi_{2-x}Sr_{2+x}Nb_{2+x}Ru_{1-x}O_{12}$, $x = 0.5$, in $I4/mmm$ symmetry with anisotropic ADPs and $B2cb$ symmetry with isotropic ADPs. The cations are shown in grayscale with white axes, strontium in light gray, bismuth in black and niobium and niobium/ruthenium in gray. The oxygen anions are shown in dark gray (red in the electronic version) with black axes. The sites are labeled according to refinements. Note that Bi_2/Sr_2 is a split site with occupancies shown in table 1. The O5 site in the $I4/mmm$ symmetry is split into the O5 and O6 sites in $B2cb$ symmetry.

Table 1. Final parameters for $Bi_{2-x}Sr_{2+x}Nb_{2+x}Ru_{1-x}O_{12}$, $x = 0.5$, from Rietveld refinement of low-temperature NPD data collected at 1.49 Å. Space group $B2cb$, $a = 5.51344(19)$ Å, $b = 5.51166(28)$ Å, and $c = 33.4325(12)$ Å, with independent isotropic atomic displacement parameters. Goodness of fit = 3.76 for 68 refined parameters. Overall powder R-factors: $R_p = 0.0492$, $wR_p = 0.0606$.

Site and occupancy for mixed site	x	y	z	$100U_{iso}$
Sr(1)	0.1056(28)	0.0047(19)	0.06265(10)	1.75(6)
0.75 Bi(2)	0.1118(25)	−0.0047(18)	0.21570(12)	1.98(7)
0.25 Sr(2)	0.1118(25)	−0.0047(18)	0.20352(46)	1.98(7)
0.5 Ru(1)	0.1014(27)	0	0.5	1.32(9)
0.5 Nb(1)	0.1014(27)	0	0.5	1.32(9)
Nb(2)	0.1078(24)	−0.0012(18)	0.37350(8)	1.71(6)
O(1)	0.8073(55)	0.2969(20)	0.00093(66)	2.18(11)
O(2)	0.3560(29)	0.2506(39)	0.24874(47)	2.12(8)
O(3)	0.0992(28)	0.0168(24)	0.44197(9)	1.84(12)
O(4)	0.1048(31)	−0.0256(27)	0.31982(13)	3.10(18)
O(5)	0.3643(25)	0.2579(21)	0.11578(30)	0.95(18)
O(6)	0.3417(26)	0.2371(24)	0.88161(38)	2.62(30)

Table 2. Comparison of refinement statistics between $I4/mmm$ and $B2cb$ symmetry. The samples with (*) contain minor impurities.

Sample	Phase symmetry	wR_p	R_p	χ^2	R_F^2
$Bi_2Sr_2Nb_2TiO_{12}$	$I4/mmm$	8.05	6.27	4.01	9.97
$(x = 0)$	$B2cb$	6.21	4.88	2.41	4.48
$Bi_{2-x}Sr_{2+x}Nb_{2+x}Ti_{1-x}O_{12}$	$I4/mmm$	8.25	6.69	2.47	11.24
$(x = 0.5)$	$B2cb$	7.30	5.98	1.95	6.18
$Bi_{2-x}Sr_{2+x}Nb_{2+x}Ru_{1-x}O_{12}$	$I4/mmm$	8.47	6.61	4.23	8.96
$(x = 0.5)$	$B2cb$	6.06	4.93	2.19	3.76
$Bi_{2-x}Sr_{2+x}Ta_{2+x}Ru_{1-x}O_{12}$	$I4/mmm$	7.17	5.64	3.21	8.94
$(x = 0.4)$	$B2cb$	5.61	4.53	1.98	4.10
$Bi_{2-x}Sr_{2+x}Nb_{2+x}Mn_{1-x}O_{12}$	$I4/mmm$	22.59	14.07	25.22	22.21
$(x = 0.4)^*$	$B2cb$	21.70	13.70	23.51	17.60
$Bi_{2-x}Sr_{2+x}Ta_{2+x}Mn_{1-x}O_{12}$	$I4/mmm$	13.45	9.67	7.37	11.20
$(x = 0.5)^*$	$B2cb$	12.62	9.11	6.55	7.08

For each sample, the structures were then Rietveld-refined against NPD data in both $I4/mmm$ and $B2cb$ symmetry for comparison. In order to maintain consistency the same background parameters and peak profile functions were used in each case. Isotropic ADPs were refined independently for each site. The cation occupancies and constraints were identical to those determined using synchrotron x-ray

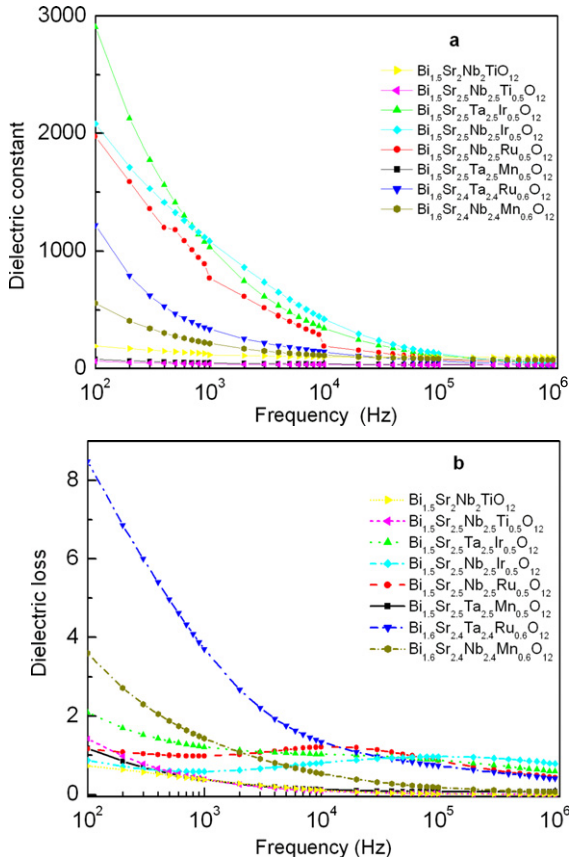

Figure 3. Plots of the (a) dielectric constant versus frequency and (b) dielectric loss tangent versus frequency for the samples.

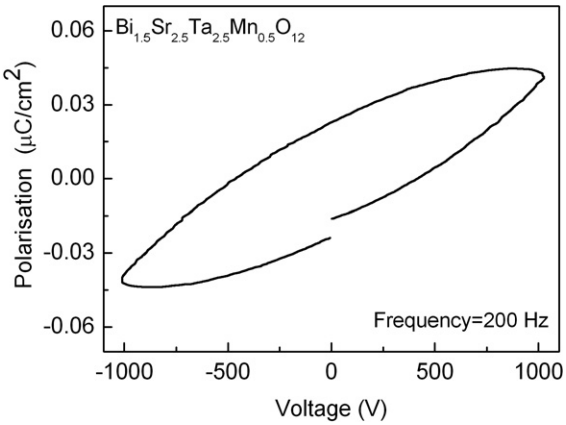

Figure 4. The ferroelectric hysteresis loop of the $Bi_{1.5}Sr_{2.5}Ta_{2.5}Mn_{0.5}O_{12}$ sample at room temperature with an applied AC electrical field of frequency 200 Hz.

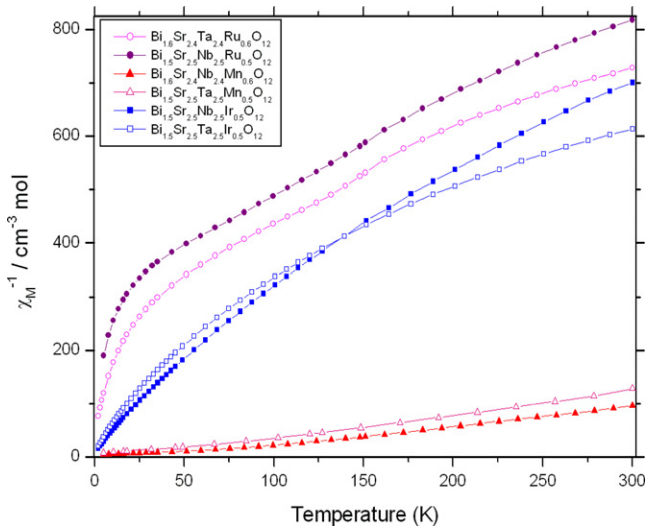

Figure 5. Plots of inverse magnetic susceptibility versus temperature for Aurivillius phases containing M = Ru (circles), Mn (triangles), and Ir (squares). B = Nb data are plotted as solid shapes, and B = Ta data are plotted as open shapes.

diffraction data [9, 12]. As no synchrotron x-ray diffraction work has been undertaken for $Bi_{1.5}Sr_{2.5}Nb_{2.5}Ti_{0.5}O_{12}$ the cation occupancies were modeled on the magnetic-cation-substituted samples. The major difference between the refinements was therefore the use of 18 structural parameters in $I4/mmm$ symmetry compared to 42 in $B2cb$ symmetry. There is a clear improvement in the fits (table 2) for all the samples in $B2cb$, that cannot be entirely attributed to the increase in the number of structural parameters, as shown by Zhou *et al* [12] for $Bi_2Sr_2Nb_2TiO_{12}$. Furthermore, an observed peak is found to be fitted in $B2cb$ symmetry that is space group forbidden in $I4/mmm$ symmetry, justifying the lowering in symmetry.

The dielectric properties of the magnetic-cation-substituted phases were compared to those of $Bi_{2-x}Sr_{2+x}Nb_{2+x}Ti_{1-x}O_{12}$, $x = 0$, 0.5, which are also expected to show evidence of an orthorhombic distortion. Figure 3 shows the dielectric constant and dielectric loss against frequency for all the samples studied at room temperature. In figure 4 the hysteresis loop of $Bi_{1.5}Sr_{2.5}Ta_{2.5}Mn_{0.5}O_{12}$ is illustrated and this sample shows a remnant polarization of 0.023 mC cm^{-2} and a coercive field of 2.5 kV cm^{-1} under the action of AC electrical field with a frequency of 200 Hz. The other samples showed similar ferroelectric hysteresis loops.

Magnetic susceptibility data were collected for all the magnetic-cation-substituted samples. Plots of inverse susceptibility versus temperature are shown in figure 5. No evidence was found in low-temperature NPD data for long-range magnetic ordering in the Ru- or Mn-containing samples.

4. Discussion

Ferroelectricity in these Aurivillius phases arises due to cation displacements and BO_6 octahedral rotations about the y axis in the perovskite-type block. These rotations in turn lower the symmetry from a tetragonal space group (e.g. $I4/mmm$) to an orthorhombic space group (e.g. $B2cb$). This particular orthorhombic space group was chosen to permit coherent displacements of cations relative to their coordinating anions and octahedral rotations (figure 2), which must be present according to the dielectric and ferroelectric results. However, since the symmetry lowering was subtle, the magnitude of the octahedral rotations is expected to be weak. In the current study the emphasis lies in proving the existence of lower

Table 3. Average ionic radii of the B-sites for all the Nb-containing samples. (Note: the ionic radii are derived from Shannons' tables [15] for the metals in six coordination. $Nb^{5+} = 0.64$ Å (also Ta^{5+}), $Ti^{4+} = 0.605$ Å, $Mn^{4+} = 0.53$ Å, $Ru^{4+} = 0.62$ Å, $Ir^{4+} = 0.625$ Å.)

Sample	B1 ionic radii (Å)	B2 ionic radii (Å)
$Bi_2Sr_2Nb_2TiO_{12}$	(0.66)Nb(0.33)Ti	(0.66)Nb(0.33)Ti
($x = 0$)	0.628	0.628
$Bi_{1.5}Sr_{2.5}Nb_{2.5}Ti_{0.5}O_{12}$	(0.83)Nb(0.16)Ti	(0.83)Nb(0.16)Ti
($x = 0.5$)	0.634	0.634
$Bi_{1.5}Sr_{2.5}Nb_{2.5}Ir_{0.5}O_{12}$	(0.5)Nb(0.5)Ir	Nb
($x = 0.5$)	0.633	0.64
$Bi_{1.5}Sr_{2.5}Nb_{2.5}Ru_{0.5}O_{12}$	(0.5)Nb(0.5)Ru	Nb
($x = 0.5$)	0.63	0.64
$Bi_{1.6}Sr_{2.4}Nb_{2.4}Mn_{0.6}O_{12}$	(0.4)Nb(0.6)Mn	Nb
($x = 0.4$)	0.574	0.64

symmetry and its associated physical properties. Octahedral rotations in perovskites arise due to a size mismatch between 12-coordinate A- and six-coordinate B-site cations, where the B-site cation is larger than optimal. The A-site cation in all our samples is Sr, while the B-site cations vary. The differences in the (average) ionic radius (IR) of B can be related to the dielectric properties of our samples. It should be pointed out that there are two distinct B-site cations in the perovskite-type block of an $n = 3$ Aurivillius phase (see figure 2)—B1 in the central layer and B2 in the outer layers. The B1 site, which lies on a mirror plane and has a much more regular coordination environment, was shown by synchrotron XRD data [9] to be preferentially occupied by the magnetic M cations ($M = Ru^{4+}$, Ir^{4+}, Mn^{4+}). Non-magnetic M cations ($M = Ti^{4+}$), however, show no preference for the B1 or B2 sites [5]. Average IRs of the B1 and B2 sites for the $B = Nb^{5+}$ samples are presented in table 3 (note that $IR(Nb^{5+}) = IR(Ta^{5+}) = 0.64$ Å [15], so the below arguments apply equally to the $B = Ta^{5+}$ samples).

We first compare the magnetic-cation-substituted samples to the non-magnetic ferroelectric $Bi_{2-x}Sr_{2+x}Nb_{2+x}Ti_{1-x}O_{12}$, $x = 0$–0.5, samples, between which there is only a very slight increase in the average IR on both the B-sites. The substitution should therefore have only a small influence on dielectric loss, and indeed the only difference between the two samples is a slightly higher dielectric loss at low frequency for $x = 0.5$ (figure 3), while they are quite similar in the high frequency range (0.0063 for $x = 0.5$ and 0.0058 for $x = 0$ at 1 MHz). The dielectric constant for $x = 0$ is three times higher than for $x = 0.5$ (97 and 33 at 1 MHz, respectively) due to higher Ti content in the B1 site.

We can then compare the $x = 0.5$ samples. Comparing $M = Ti^{4+}$ to $M = Ru^{4+}$ and Ir^{4+}, a very slight difference is observed in the average IR of the two B-sites, but for $M = Mn^{4+}$ the IR in the B1 site is quite small. However, from figure 3(a), the Ir-doped samples have the highest dielectric constant, followed by the Ru-doped samples and then the Mn-doped samples, which are on a par with the Ti-doped samples. The addition of magnetic cations that are similar in IR to Ti^{4+} therefore increases the dielectric constant; i.e., they enhance the ability for the B2 sites to polarize. With a smaller cation $M = Mn^{4+}$, the majority of the polarizability of the B2 sites can be attributed to the remaining Nb^{5+} on the B1 site, similar to the $M = Ti^{4+}$ $x = 0.5$ sample.

The similarity of the dielectric constants in the higher frequency range suggests the observed difference in dielectric constant at lower frequency is a non-intrinsic effect. Moreover, in all the $x = 0.5$ samples a weak, but broad, dielectric loss peak is evident as shown in figure 3(b), probably due to structural disorder or the formation of local space charge fields due to the different sizes and negativities of cations in the B1 site (i.e. relaxor ferroelectric behavior). In the $x = 0.4$ samples, significantly higher dielectric losses are shown at lower frequency, indicating even stronger structural disordering or distortion. The internal strain could not be quantified as the strain values were within the experimental error of the cell parameters. However, the hypothesis of increased internal strain is consistent with $x = 0.4$ being the lowest value of x that we could experimentally achieve for magnetic-cation-doped Aurivillius phases.

The dielectric results show the similarities between the non-magnetic- and magnetic-cation-doped samples. The correlation between the Rietveld-refined fits to NPD data in orthorhombic $B2cb$ symmetry with the physical properties of the synthesized materials is further evident by the ferroelectric hysteresis loop for $Bi_{1.5}Sr_{2.5}Ta_{2.5}Mn_{0.5}O_{12}$, shown in figure 4. The samples exhibit weak remnant polarization that corresponds to the symmetry lowering. The magnitude of the remnant polarization is low, since the magnitudes of the octahedral distortions on the B2 sites were low and careful analysis of NPD was required to confirm the symmetry lowering. Nevertheless, the observation of the hysteresis loops shows that the synthesized compounds are ferroelectric.

A multiferroic (ferroelectromagnetic) Aurivillius phase needs to exhibit long-range ferromagnetism and ferroelectric properties. The synthesized ferroelectric compounds show no evidence for long-range magnetic order in the low-temperature NPD data, but the magnetic susceptibility data presented in figure 5 indicate that the presence of ∼50% magnetic cations in the central B1 octahedral layer does lead to short-range magnetic interactions. For the smaller cation M = Mn, the data provide evidence for ferromagnetic exchange with quite low Curie temperatures $T_C \approx 50$ K (B = Nb) and $T_C \approx 25$ K (B = Ta). Spin–orbit coupling dominates in the case of the larger M = Ru and Ir, although for M = Ru there is an indication of antiferromagnetic exchange at low temperature.

Magnetic-cation-doped $n = 3$ Aurivillius phases therefore present promising signs of magnetic exchange within the central corner-shared layer of BO_6 octahedra, given that only a maximum of 60% (where $x = 0.4$) of these B1 sites are occupied by magnetic cations. What is particularly interesting and promising, however, is that the substitution of magnetic Ru^{4+}, Ir^{4+} and Mn^{4+} for non-magnetic Ti^{4+} cations at a given $x = 0.5$ actually improves the dielectric polarization. Various synthetic routes are now being explored with the aim of reducing the minimum value of x to 0, creating a fully magnetic 2D layer of corner-sharing MO_6 octahedra sandwiched between ferroelectric layers.

5. Conclusions

We have shown by the careful analysis and Rietveld refinement of neutron powder diffraction (NPD) data that magnetic-cation-doped three-layer Aurivillius phases $Bi_{2-x}Sr_{2+x}(Nb/Ta)_{2+x}M_{1-x}O_{12}$, $x \approx 0.5$ and $M = Ru^{4+}$, Ir^{4+} or Mn^{4+} have orthorhombic $B2cb$ space group symmetry, and are ferroelectric. They are structurally analogous to their (non-magnetic) ferroelectric parent compound $Bi_{2-x}Sr_{2+x}Nb_{2+x}Ti_{1-x}O_{12}$, $x = 0, 0.5$, with which they also share similar dielectric properties. Furthermore, the dielectric polarization when $x = 0.5$ appears to be enhanced by the presence of magnetic transition metal cations versus non-magnetic Ti^{4+}, possibly because of the preferential location of all the magnetic cations on the central B1 octahedral site creating a higher degree of local strain and disorder.

The magnetic-cation-doped phases also show evidence for short-range ferromagnetic (M = Mn) and antiferromagnetic (M = Ru and Ir) exchange, demonstrating the potential of these naturally layered phases as templates for multiferroic (magnetoelectric) materials. The phases with partially magnetic-cation-doped layers ($x > 0$) exhibit local magnetic exchange which might become long range if these layers could be completely filled ($x = 0$), and synthetic efforts to achieve this goal are ongoing in the hope that these phases can be developed into a tunable class of multiferroics (magnetoelectrics).

Acknowledgments

The neutron powder diffraction work was supported by the Australian Institute of Nuclear Science and Engineering (AINSE) under AINGRA06246. We wish to thank Dr Q Zhou for the preparation of the $Bi_2Sr_2Nb_2TiO_{12}$ compound, Dr M Avdeev for some NPD data collection and Dr B. Moubaraki for collecting magnetic susceptibility data. BJK and CDL acknowledge the support of the Australian Research Council.

References

[1] Aurivillius B 1949 *Ark. Kemi.* **1** 463
[2] Aurivillius B 1950 *Ark. Kemi.* **2** 519
[3] Subbarao E C 1962 *J. Phys. Chem. Solids* **23** 665
[4] Smolenski G A, Isupov V A and Agranovskaya a I 1953 *Sov. Phys.—Solid State* **3** 651 (Engl. Transl.)
[5] Hervoches C H and Lightfoot P 2000 *J. Solid State Chem.* **153** 66
[6] Ismailzade I G, Nesteren V I, Mirishli F A and Rustamov P G 1967 *Sov. Phys. Cryst.* **12** 400
[7] Hervoches C H, Snedden A, Riggs R, Kilcoyne S H, Manuel P and Lightfoot P 2002 *J. Solid State Chem.* **164** 280
[8] Snedden A, Hervoches C H and Lightfoot P 2003 *Phys. Rev.* B **67** 92102
[9] Sharma N, Ling C D, Wrighter G E, Chen P Y, Kennedy B J and Lee P L 2007 *J. Solid State Chem.* **180** 370–6
[10] Yu W J, Kim Y I, Ha D H, Lee J H, Park Y K, Seong S and Hur N H 1999 *Solid State Comm.* **111** 705
[11] Tripathy M, Mani R and Gopalakrishnan J 2007 *Mater. Res. Bull.* **42** 950–960
[12] Zhou Q, Kennedy B J and Elcombe M M 2006 *J. Solid State Chem.* **179** 3744–3750
[13] Larson A C and Von Dreele R B 1994 General structure analysis system (GSAS) *Los Alamos National Laboratory Report* LAUR 86-748
[14] Toby B H 2001 *J. Appl. Crystallogr.* **34** 210
[15] Shannon R D 1976 *Acta Crystallogr.* A **32** 751–67